Available online at www.sciencedirect.com
ScienceDirect
Journal of the European Ceramic Society 32 (2012) 195–202
www.elsevier.com/locate/jeurceramsoc

Electrical creep around a circular hole in PLZT 8/65/35

Q.D. Liu [a,*], J.E. Huber [b]

[a] MOE Key Laboratory for Strength and Vibration, Xi'an Jiaotong University, Xi'an 710049, PR China
[b] Department of Engineering Science, University of Oxford, Parks Road, Oxford OX1 3PJ, UK

Received 10 April 2011; received in revised form 26 July 2011; accepted 6 August 2011
Available online 27 August 2011

Abstract

The strain–birefringence correlation was exploited to study the local behaviour near a circular hole in unpoled PLZT 8/65/35 under electric field below than the coercive field. The observed birefringence contours near the hole show a spatial distribution and time dependence. Due to the enhancement of electric field near the hole, the polarization creep rate is greatly increased. The evolution of the local principal strain difference with time and position in the sample is quantified. Overall, an accelerated poling effect is found in comparison with the behaviour under uniform field. This appears to be due to inhomogeneous field distribution which initiates polarization switching in areas of locally enhanced electric field. The presence of the hole promotes a nearly linear growth in average polarization with time, despite the strongly nonlinear response of the parent material. The results indicate that insulating porosity can strongly affect the switching behaviour and coercivity of ferroelectric ceramics.

Keywords: Ferroelectric properties; PLZT; Birefringence; Circular hole; Stress concentration; Electric boundary condition

1. Introduction

Ferroelectric ceramics creep when subjected to steady electric field or stress conditions. While this effect can be ignored in some applications, it presents a difficulty in engineering design, for example in developing reliable precision actuators.[1] Experimental observations show that time dependent, or creep, effects are significant for some compositions of bulk ferroelectrics.[2–4] The dominant mechanism appears to be a gradual motion of domain walls, giving rise to changes in both irreversible strain and electrical polarization. However, there are relatively few studies of creep effects in these materials.

Transparent ferroelectrics such as PLZT 8/65/35 provide the opportunity to study creep strain fields using birefringence methods. PLZT ceramics have coupling of electrical, mechanical and optical properties that make them effective in various engineering applications.[5–8] Photoelastic methods for studying the stress-optical and electro-optical behaviour are well established.[9–11] A major advantage of this approach arises when studying non-uniform field conditions, in that the spatial variation of strain can be captured in birefringence images. Local strain measurements using strain gauges have provided valuable information on material rate effects[3,4] that can be used for material modelling and also to calibrate birefringence strain measurements. Birefringence methods then provide a way to measure the spatial variation of the non-uniform fields that arise near features such as internal electrodes, defects, cracks and other geometric features. Understanding the effect of such features on both the static and the time dependent material response is important to device design. In the literature, theoretical and experimental work has been carried out concerning various types of inhomogeneity, especially cracks and embedded electrodes.[12–19] In the present work we focus on the electrical creep fields around an insulating circular hole.

The study of ferroelectric response in the vicinity of a circular hole (or inclusion) is motivated by both theoretical and practical considerations. It is well known that the porosity in sintered electroceramics affects their properties. Enhancement of porosity by artificial pore formers is used to reduce transformation stress and modify elastic, dielectric or piezoelectric response in transducer materials.[20–22] The effect of porosity has generally been studied using bulk measurements or diffraction techniques.[21,23] In the present work we observe the effect of a single hole, representative of the local inhomogeneity due to an insulating pore or inclusion. A 2-dimensional geometry is used to enable spatially resolved measurements by birefringence

* Corresponding author. Tel.: +86 29 82663657; fax: +86 29 82663657.
E-mail address: qdliu@mail.xjtu.edu.cn (Q.D. Liu).

0955-2219/$ – see front matter © 2011 Elsevier Ltd. All rights reserved.
doi:10.1016/j.jeurceramsoc.2011.08.008

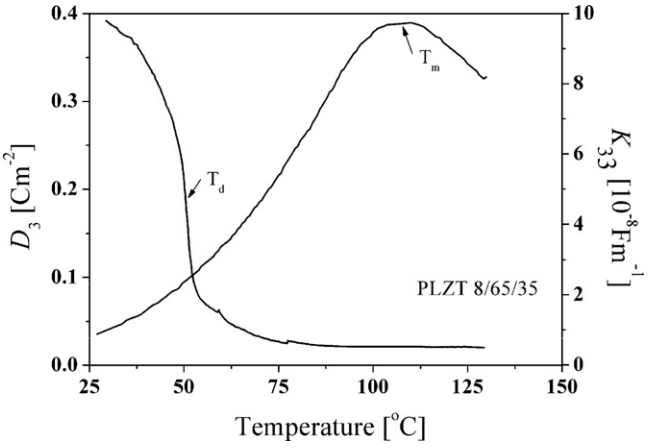

Fig. 1. Temperature dependence of dielectric permittivity κ_{33} and electric displacement D_3.

methods. A similar geometry was modelled using a viscoplastic model by Belov and Kreher.[24] They found that by allowing 90° and 180° switching among a set of 42 domain orientations, typical polycrystalline ferroelectric behaviour could be reproduced. From the point of view of theoretical modelling, the measurements provide non-linear creep data that can be used to test models of the coupled electromechanical response of ferroelectrics and to test the suitability of the impermeable or exact surface boundary conditions for an open pore-like flaw.[25–30]

2. Experimental

2.1. Birefringence measurement in PLZT 8/65/35

Bulk PLZT 8/65/35 ceramic with grain size about 1 μm was used in the as-sintered (unpoled) state. The composition lies close to the boundaries of cubic (non-polar), tetragonal, rhombohedral and orthorhombic phases on the phase diagram for PLZT system at room temperature.[10,31] The material is optically transparent in the unpoled state and undergoes a transition to a strongly scattering or opaque state when poled.[32] On the PLZT phase diagram, the boundaries of cubic (non-polar), tetragonal, rhombohedral and orthorhombic phases[31] of this composition show relaxor behaviour. The bulk material behaviour was checked by measuring the low frequency temperature ($T_m \sim 110\,^{\circ}C$) of peak permittivity (κ_{33}) and the thermal depoling behaviour ($T_d \sim 55\,^{\circ}C$) as shown in Fig. 1. The temperature dependence of the dielectric hysteresis and butterfly hysteresis were also checked. A low frequency (0.1 Hz) coercive field $E_c = 0.4\,MV\,m^{-1}$, and a saturation polarization $D_0 = 0.32\,cm^{-2}$ were found. The material behaviour is in good agreement with measurements from other researchers.[33–35]

Ferroelectric crystals are optically anisotropic below the Curie temperature (T_c) and hence have intrinsic birefringence. There are also several sources of extrinsic birefringence in PLZT 8/65/35, corresponding to external influences that cause anisotropy such as the electro-optical or photoelastic effects.[7,9] Simple models include the linear electro-optic (or Pockels) coefficient, the quadratic electro-optic (or Kerr) coefficient, and the strain-optical coefficients or the quadratic effect; higher order terms are usually negligible under conditions of small strain and electric field. Since the speed of light depends on the electron density, the difference in refractive index between two principal directions, $\Delta n = |n_1 - n_3|$, is closely related to the principal strain difference ($\varepsilon_{11} - \varepsilon_{33}$), giving rise to standard procedures of photoelastic strain measurement.[9] When light of wavelength λ passes through a specimen of thickness t, orthogonal plane polarized waves experience a relative phase difference

$$\delta = \frac{2\pi t \Delta n}{\lambda}. \tag{1}$$

Birefringence measurements in the present work are carried out using an automated rotating polariser method in the Metripol microscope.[36] The optical path of the Metripol microscope consists of a rotating polarizer, the material specimen, a quarter wave plate and an analyser. With the polarizer at specific angular position, α_i ($i = 1, 2, \ldots, 5$), the transmitted light intensity I is given by Glazer et al.[36]:

$$I = \frac{I_0}{2}\{1 + \sin\delta \sin 2(\varphi - \alpha_i)\},$$
$$\varphi = \tan^{-1}(n_1/n_3). \tag{2}$$

where $I_0/2$ is the mean transmitted light intensity and φ is the orientation angle of the optical indicatrix, corresponding to the orientation of the fast optical axis. By rotating the polarizer to several angles ($0 \le \alpha_i \le \pi$), and recording light intensity, $|\sin\delta|$, φ and $I_0/2$ are calculated at each point in the field of view using an automated analysis. As a gradual loss of transparency, and hence measurement sensitivity, accompanies the increase of polarization in PLZT 8/65/35, direct use was made of the signal from the 8-bit CCD camera (8-bits) used to collect images in the Metripol system and analyse them following the methods of Liu et al.[19] By varying the sample thickness t and wave length λ, the refractive index n_0 of PLZT 8/65/35 in the unpoled state was measured to be approximately 2.55, and a change in Δn of about 0.025 was found between the unpoled and the fully poled state.

2.2. Homogeneous electrical creep measurements

In previous work of Liu et al.[19] measurements on bulk PLZT 8/65/35 ceramic were used to establish a correlation between birefringence Δn and strain under uniform electric field conditions. A brief description is included here for clarity in the later sections where this correlation is used. Specimens of size 8.6 mm × 5 mm × 0.36 mm were produced by dicing bulk ceramic and polishing the 5 mm × 8.6 mm surfaces using 1 μm diamond paste. In order to reduce residual stresses, specimens were annealed at 300 °C for 120 min and the initial state was checked by Metripol microscope to be uniform and optically isotropic. Electrodes were made using silver loaded epoxy on the 8.6 mm × 0.36 mm faces and the low voltage side was connected to a 2.96 μC capacitive electrometer. The strains ε_{33} in the applied electric field direction, and ε_{11} perpendicular to the applied field were monitored with strain gauges, while the birefringence ($\Delta n = n_1 - n_3$) was deduced from the $|\sin\delta|$ measurements of the Metripol microscope in a region of material

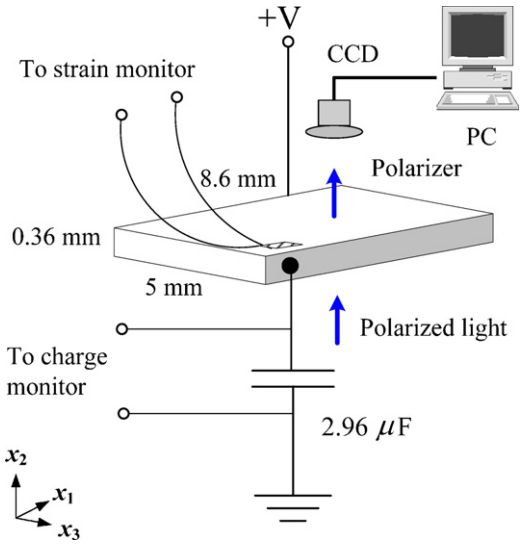

Fig. 2. Schematic of the PLZT 8/65/35 specimen in the charge–strain–birefringence measurement system.

2.8 mm × 1.8 mm in size near the specimen centre (see Fig. 2). Each specimen was immersed in oil in a glass dish to reduce the risk of arcing and stabilize temperature. The optical isotropy of the system was checked both with and without the PLZT specimen in the light path.

The polarization and strain fields $D_3(t)$, $\varepsilon_{33}(t)$, and $\varepsilon_{11}(t)$ were measured while the initially unpoled sample was subjected to a constant electric field E_3, produced by a voltage signal with a rapid rise (about 10 ms) followed by a constant voltage for 300 s. A linear correlation between principal strain difference and birefringence was found, as shown in Fig. 3.

2.3. Electrical creep around a circular hole

Blocks of PLZT 8/65/35 were drilled with a 1 mm centre hole ($r_0 = 0.5$ mm) and then sliced to produce specimens with dimensions of 8.6 mm × 5.0 mm × 0.5 mm. After polishing with

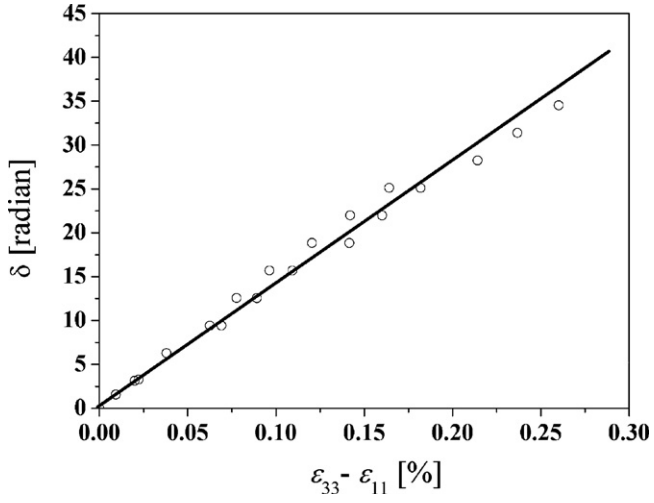

Fig. 3. Birefringence phase difference δ versus principal strain difference ($\varepsilon_{33} - \varepsilon_{11}$) as shown by Liu et al.[19]

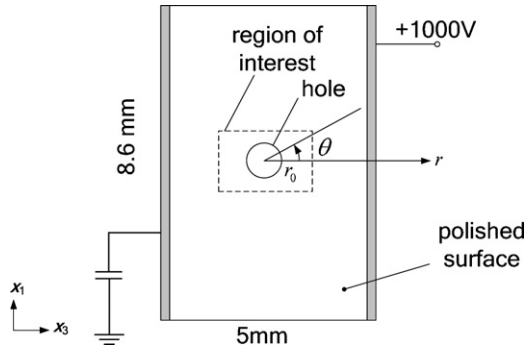

Fig. 4. General arrangement of the PLZT 8/65/35 specimen with a hole (diameter $2r_0 = 1.0$ mm).

1 μm diamond paste, and annealing, the specimen thickness was 0.36 mm. Electrodes were applied and a specimen was connected into the loading circuit and mounted with the Metripol microscope focussed on a 1.8 × 2.8 mm region of interest (see Fig. 4).

A constant 1000 V was applied across the electrodes, giving a mean electric field of $0.5E_c$ in the negative x_3 direction, corresponding to $\theta = \pi$ in the polar coordinate system of Fig. 4. The hole geometry produces non-uniform electric field and consequently non-uniform ferroelectric switching close to the hole.

Fig. 5 shows a series of birefringence images indicating the measured $|\sin\delta|$ and φ values in the region of interest after various time intervals up to 600 s after the voltage was applied. The $|\sin\delta|$ data were first reported in our previous work.[37] In the present study the data are analysed to gain further insight. Each image shows data collected over an 8 s interval in which the polariser was rotated. Images are shown in a vertical series corresponding to the state just before the voltage was applied (0 s) and then 8 s, 32 s, 120 s, and 600 s after the application of the constant voltage. The measurements clearly demonstrate that creep occurs under constant voltage loading with the mean field well below the coercive level. Although care was taken to eliminate polishing scratches and to relieve residual stresses, some inhomogeneity due to specimen processing can still be seen in the initial state, at $t = 0$ s. The Metripol microscope has very high sensitivity to strain, with strains of order 10^{-6} detectable. Consequently slight deviations from the isotropic state were detected. The initial state away from the hole had $\delta \sim 0.2$ while the hole edge had $\delta \sim 3.8$, corresponding to strains of order 10^{-4}. Due to the existence of the initial strains around the hole, two optically isotropic points appeared during subsequent loading, at radial position $r \sim 0.7$ mm with $\theta = 0$ and π; these gradually moved towards the hole as time progressed. Since these positions maintained zero order birefringence throughout, they formed a useful reference for deducing the order of birefringence of other fringes.

Fig. 6 shows the lower half of the $|\sin\delta|$ image from Fig. 5 at time $t = 600$ s. The measured values of $|\sin\delta|$ along a cross-section at $\theta = 0$ are plotted against position. It is expected that the hole has insulating behaviour with dielectric permittivity much less than that of the specimen, so almost all of the voltage drop between A′ and A occurs within the hole. Consequently the electric field is expected to be weak in region A′A of the specimen,

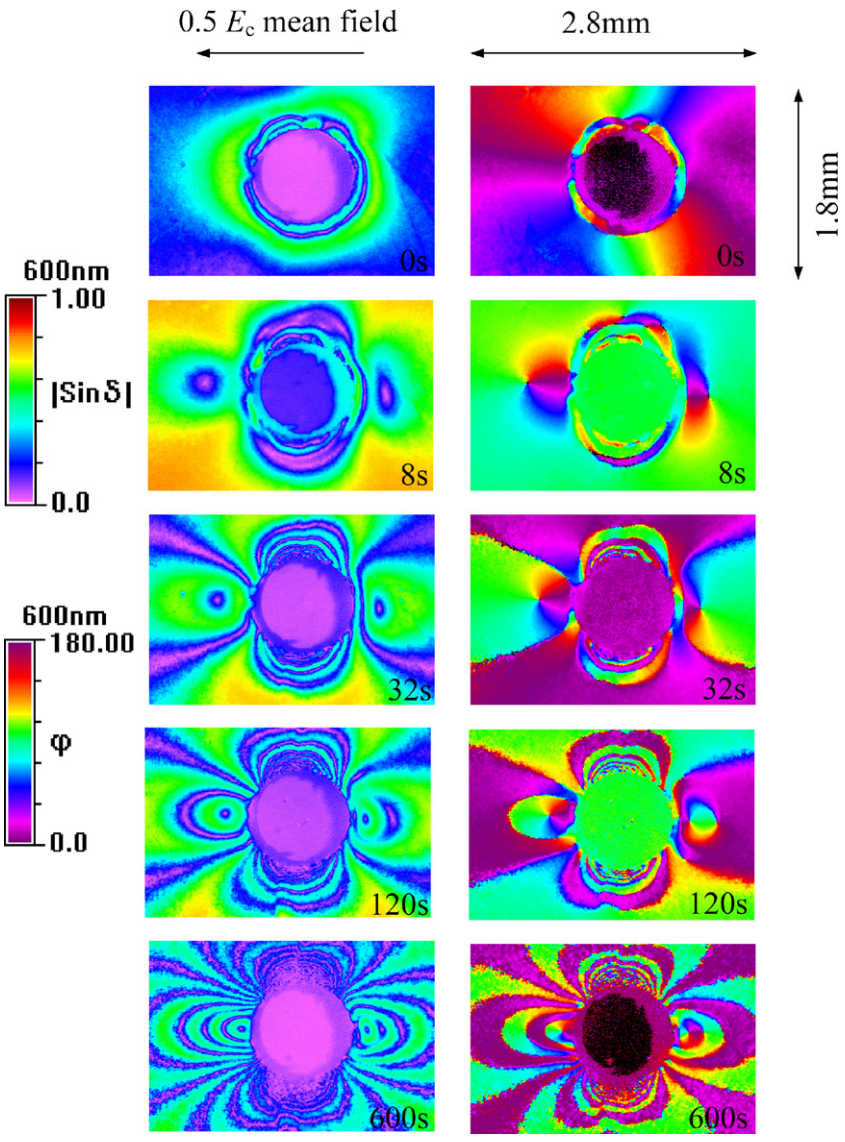

Fig. 5. Measured birefringence contours of $|\sin\delta|$ and φ evolving with time under a constant mean electric field of $0.5E_c$ for PLZT 8/65/35 with a circular hole.

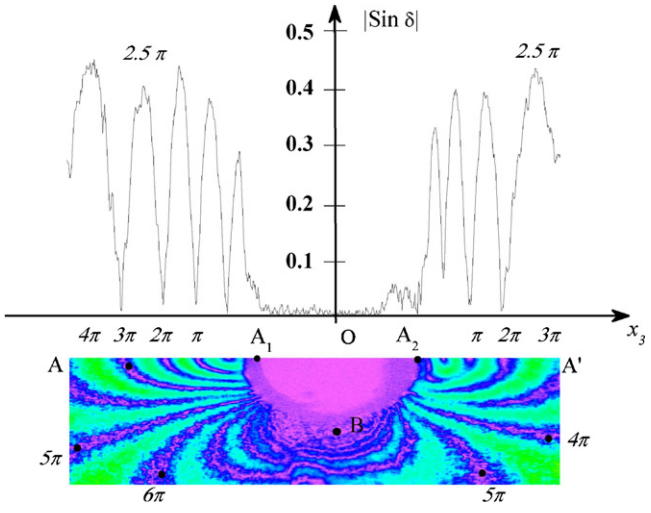

Fig. 6. Distribution of $|\sin\delta|$ along the line $\theta = 0°$ after 600 s, showing δ values at each zero of $|\sin\delta|$.

giving a low creep rate, while point B at $\theta = -\pi/2$ has elevated electric field and rapid creep. There are about five orders of birefringence along cross-section AA′ in Fig. 6. In previous work, it was shown that uniform fields less than $0.7E_c$ cause almost no creep in strain and polarization within 600 s,[19] so the birefringence contours observed here are due to the inhomogeneity caused by the hole.

By attributing the outermost fringe of the radiating fringe pattern to the first order of birefringence, with successive fringes representing higher orders, the value of principal strain difference is found at each point in the $|\sin\delta|$ image. Note that the orientation of the principal axes φ is not aligned with the global x_1 and x_3 axes, but varies throughout the region of interest due to the field concentration around the hole. Fig. 7 shows the local principal strain difference versus time at several positions around the hole. The creep rate increases with radial position r when $\theta = 0$, but decreases with r when $\theta = \pi/2$. This is consistent with the shielding of electric field at $\theta = 0$ by the low permittivity hole and the enhancement of field strength near the hole surface

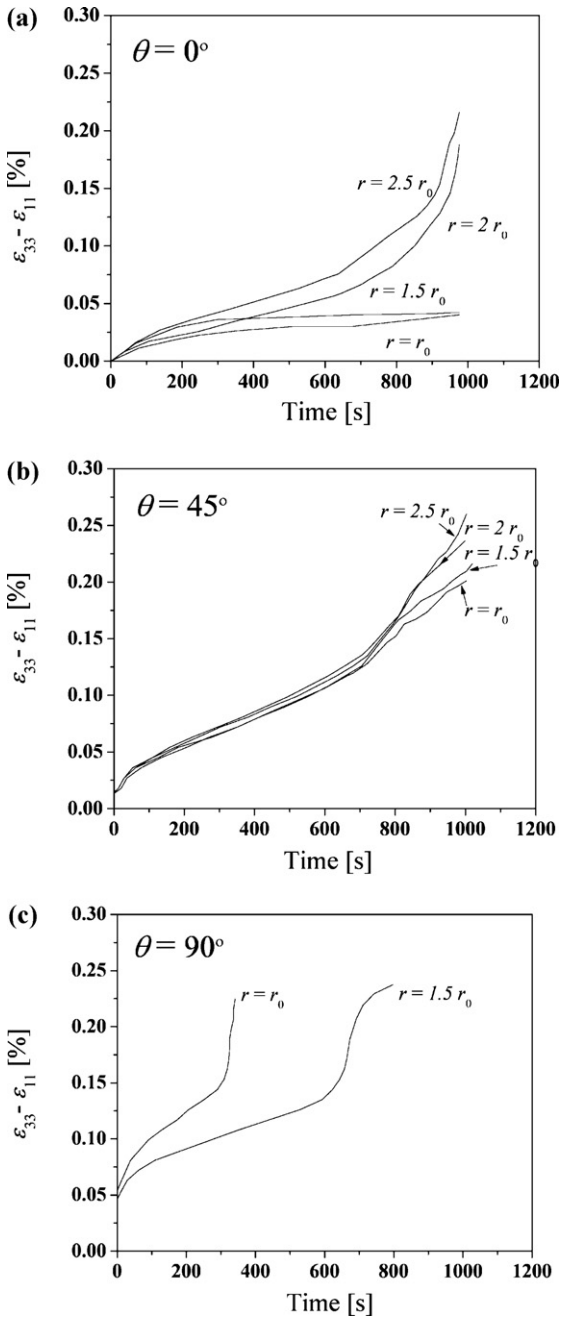

Fig. 7. The local principal strain difference versus time at various radial positions on lines at (a) $\theta = 0$, (b) $\theta = \pi/4$ and (c) $\theta = \pi/2$.

when $\theta = \pm\pi/2$. At $\theta = \pi/4$, the creep rate is almost independent of radial position. In Fig. 7c, a saturation of switching, defined by the stabilization of the principal strain difference, was observed after 360 s near the hole surface ($r = r_0$) and 720 s for $r = 1.5r_0$. Saturation was not reached at points on the $\theta = 0$ line (Fig. 7a).

The principal strain difference data are replotted in Fig. 8 to show the evolution with time at radial positions $r = 1.5r_0$ and $2r_0$. Close to the hole surface, there is strong angular dependence of strain rate, while further from the hole the angular dependence is reduced. All of these observations are qualitatively as expected for creep due to field concentration around an insulating hole or inclusion of low permittivity.

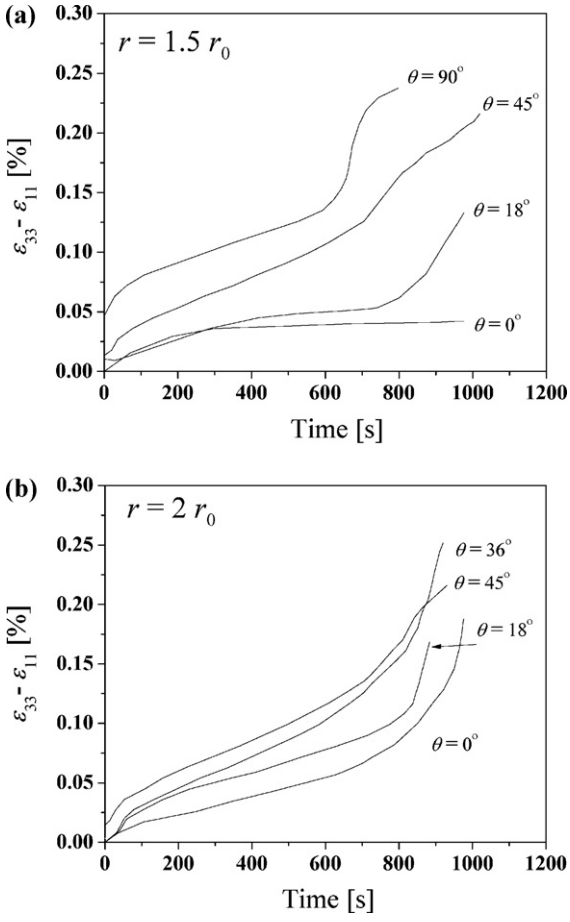

Fig. 8. Local principal strain difference data by radial position: (a) $r = 1.5r_0$ and (b) $r = 2.0r_0$.

Fig. 9 shows the average charge density $\bar{D}_3$ on the lower electrode versus time, for specimens with and without a hole, in each case subjected to a mean field of $0.5E_c$. The area around the hole produces accelerated switching by introducing non-uniform field conditions, and this effect strongly dominates the switching behaviour. In the uniform field test, the material remains almost unpolarized throughout, while the presence

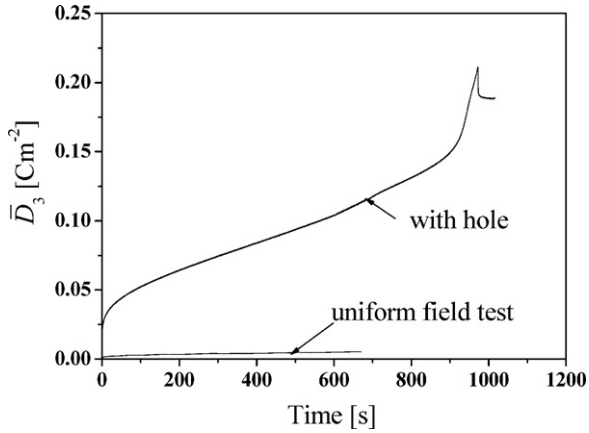

Fig. 9. The measured average electric displacement ($\bar{D}_3$) against time under a constant mean electric field of $0.5E_c$ for PLZT 8/65/35 specimens with and without a hole.

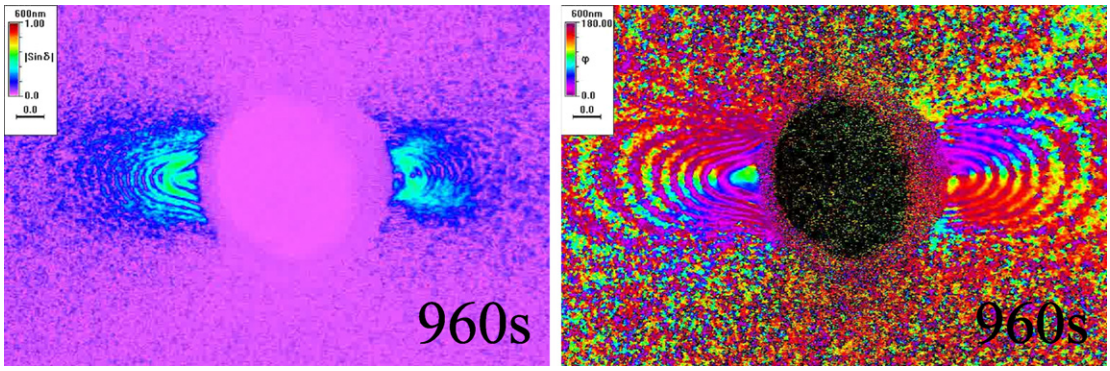

Fig. 10. Measured birefringence contours after 960 s showing saturation in the region near the hole flanks.

of the hole appears to promote a rapid increase of polarization towards the saturated state. However, the shielding effect of the hole inhibits the poling process in regions close to the hole where $\theta = 0$ or π. Consequently the sample reaches a peak mean polarization magnitude of $\bar{D}_3 \sim 0.22\,\mathrm{cm}^{-2}$, or 70% of the material saturation polarization D_0. The small drop in $\bar{D}_3$ seen in Fig. 9 after 960 s corresponds to switching off the electric field indicating that the final value of $\bar{D}_3$ is a remanent polarization.

In this material, full switching to the saturated state produces a principal strain difference $\varepsilon_{33} - \varepsilon_{11}$ of 0.25%, while the change in the principal strain difference between the adjacent fringes in the specimen was 0.018%. Thus 14 fringes are expected between unpolarized and saturated material. Referring to Figs. 5–8 it is evident that saturation has not been reached throughout most of the region of interest within 600 s. However, Fig. 10, taken after 960 s indicates that most of the region of interest is saturated by this time, except for a band of material shielded by the hole.

3. Discussions

In a linear dielectric, the presence of a circular insulating hole, of negligible permittivity and radius r_0, in a region experiencing a remote electric field in the x_3 direction $E_3 = E_\infty$, gives rise to the electric field distribution

$$E_3 = E_\infty \left(1 - \frac{r_0^2}{r^2}\cos 2\theta\right) \tag{3}$$

$$E_1 = -E_\infty \frac{r_0^2}{r^2}\sin\ 2\theta \tag{4}$$

where r and θ are the polar co-ordinates defined in Fig. 4. In the present experiment, the initial state of the material is close to isotropic, so that piezoelectric coupling is initially absent. Thus, Eqs. (3) and (4) are representative of the electric fields immediately after the constant voltage is switched on. The electric field magnitude is

$$E = |\mathbf{E}| = E_\infty \left(1 + \frac{r_0^4}{r^4} - \frac{2r_0^2}{r^2}\cos\ 2\theta\right)^{1/2} \tag{5}$$

For simplicity, we neglect the coupling that develops as the experiment progresses and assume that the creeping process is controlled by the local electric field magnitude of Eq. (5). In the early stages of switching, Liu et al.[19] found that the remanent polarization increased in a power-law relation with electric field magnitude, while the principal strain difference developed quadratically with the total electric displacement. Given the linear relationship between principal strain difference and birefringence, an estimate of the optical phase shift δ in the early stages of creep due to electrical loading is

$$\delta = \left(\alpha\left(\frac{E}{E_\mathrm{c}}\right) + \beta\left(\frac{E}{E_\mathrm{c}}\right)^m t\right)^2 + \delta_0 \tag{6}$$

where α, β and m are constants. The first term in Eq. (6) captures the linear dielectric effect, while the second accounts for creeping polarization with time. The final term, δ_0, is included to allow for the initial distribution of birefringence, present before electric field is applied. In our experiment, this initial distribution can be represented approximately by

$$\delta_0 = 0.2 + 3.6\left(\frac{r_0}{r}\right)^4 \tag{7}$$

The evolution of birefringence due to Eq. (6) is illustrated in Fig. 11, using the parameters $\alpha = 4$, $\beta = 0.5$ and $m = 6$. The power law exponent m is governed by the kinetics of domain growth and is temperature dependent; an analysis of the kinetics has been given by Belov and Kreher.[38] In soft PZT ceramics, a value of m around 22 at room temperature was found, consistent with thermal activation of the switching mechanism.[4,39] In PLZT 8/65/35 the behaviour is more complex due to the presence of separate process of domain nucleation and switching,[19] and the value $m = 6$ is used here as an approximation of the overall behaviour. An improved model could be developed through consideration of the kinetics of the separate processes of nucleation and switching.

The gradual loss of transparency that accompanies increasing polarization in PLZT 8/65/35[19] distorts the measured $|\sin\delta|$ values, and this is simulated in Fig. 11 by scaling $|\sin\delta|$ by $1 - (\delta/14\pi)$. Note that this scaling makes the colour mapping of the fringes consistent with the experimental data, but does not affect the fringe positions.

Fig. 11 qualitatively captures several of the effects seen in the experimental $|\sin\delta|$ data of Fig. 5. At time $t = 0$, the initial state approximated by Eq. (7) is illustrated. Then, after 8 s with the electric field is switched on, the $|\sin\delta|$ image shows a few

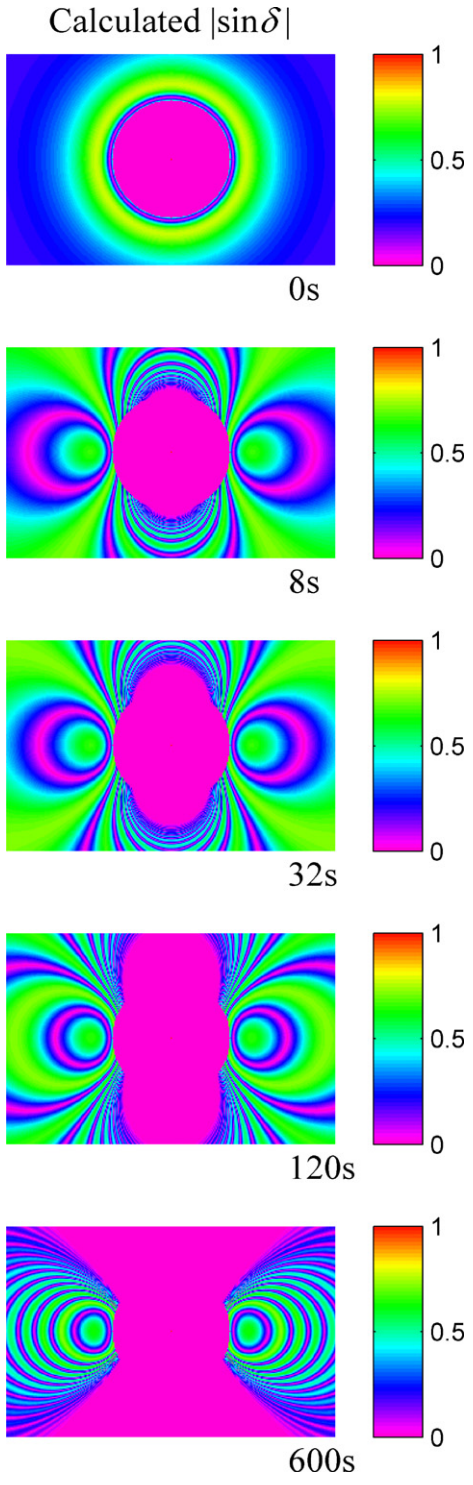

Fig. 11. Birefringence contours of $|\sin\delta|$ calculated using Eq. (6).

fringes, concentrated around the flanks of the hole ($\theta = \pm\pi$). Eq. (6) predicts an electric field strength of $2E_\infty$ when $r = r_0$ and $\theta = \pm\pi/2$; this results in the flanks of the hole experiencing electric field equal to the coercive field and consequently a saturated state is rapidly reached in these regions. As time progresses the saturated region spreads around the hole, driving fringes ahead of it until after 600 s two triangular regions delimited roughly by $\pi/4 < |\theta| < 3\pi/4$ are close to the saturated state. As in the experiment, the region around $\theta = \pm\pi$ remains only partially polarized after 600 s. Eq. (6) gives qualitatively similar response to the experiment, and is thus helpful in interpreting the data. However, it does not give good quantitative agreement with the experimental data. For quantitative agreement, the full material non-linearity described by Liu et al.,[19] and the coupled electromechanical response should be taken into account. At present, no material model is available to capture all of these effects. It seems, though, that the dominant effect is accelerated switching due to the non-uniform electric field, and this is captured even by the simple model described here.

In the unpoled state, PLZT 8/65/35 is a glassy, optically isotropic material which is characterised by microdomain regions that can grow into macrodomains under applied electric field.[33] The initial stage of polarization involves the nucleation and growth of macrodomains. This is followed by re-orientation of the ferroelectric domains through switching (domain wall motion). Both of these stages have a degree of rate-dependence, but the nucleation of macrodomains dominates the creep behaviour in PLZT at low field strengths. The presence of insulating pores produces locally elevated electric field levels that, in keeping with the power law dependence of polarization growth, greatly increase the rate of growth of macrodomains. This enables the specimen to be rapidly poled, although the mean field strength is well below the coercive field level. Other ferroelectrics, such as PZT ceramics, have macrodomains in the as sintered state, and so do not require this initial step. However, PZT ceramics also display power law electrical creeping behaviour[4] and so can be expected to show enhanced electrical creep rates when porosity is present. The hole in our sample is representative of a porosity of about 1.8%, which is consistent with porosity levels in imperfectly sintered electroceramics. With the use of pore-formers, an order of magnitude increase in porosity is readily achievable. Thus it should be possible to modify electrical creep behaviour through the control of porosity.

4. Conclusions

Creeping birefringence under constant voltage boundary conditions was observed in samples of PLZT 8/65/35 with and without a central hole. Using a correlation between the birefringence phase shift and principal strain difference, the evolution of the strain field around the hole was measured. The results showed that the presence of a hole greatly accelerates the overall polarization rate. With the hole present, a mean field strength of half the coercive field caused the sample to become 70% poled by creeping processes within 10^3 s. It appears likely that the local field enhancement due to the hole assists the nucleation of domains from an initially glassy (transparent) state in PLZT 8/65/35. This suggests that the presence of porosity could greatly reduce the mean field necessary to produce a polarized state in PLZT 8/65/35. Although the mechanism of polarization increase is different in non-relaxor PZT compositions, an enhancement to the switching process would still be expected, as has been observed in studies of PZT compositions with artificially elevated porosity.

Acknowledgments

This work is partly supported by the NSFC with grants of 10802062 and 10972007. The authors would like to thank Professor N. A. Fleck, and Dr D. P. Chu for the helpful discussions.

References

1. Janocha H, Kuhnen K. Real-time compensation of hysteresis and creep in piezoelectric actuators. *Sens Actuators A: Phys* 2000;**79**:83–9.
2. Guillon OF, Thiebaud F, Delobelle P, Perreux D. Compressive creep of PZT ceramics: experiments and modeling. *J Eur Ceram Soc* 2004;**24**:2547–52.
3. Zhou DY, Kamlah M. Room-temperature creep of soft PZT under static electrical and compressive stress loading. *Acta Mater* 2006;**54**:1389–96.
4. Liu QD, Huber JE. Creep in ferroelectrics due to unipolar electrical loading. *J Eur Ceram Soc* 2006;**29**:2799–806.
5. Land CE. Variable birefringence light scattering and surface-deformation effects in PLZT ceramics. *Ferroelectrics* 1974;**7**:45–51.
6. Lines ME, Glass AM. Principles and applications of ferroelectric and related materials. 1st ed. Oxford: Clarendon Press; 1977.
7. Nye JF. Physical properties of crystals: their presentation by tensors and matrices. Oxford: Oxford Science Publications, Clarendon Press; 1985.
8. Scott JF. The physics of ferroelectric ceramic thin films for memory applications Ferroelectrics. *Review* 1998;**1**:1–129.
9. ASTM-D4093-95. Standard test method for photoelastic measurements of birefringence and residual strains in transparent or translucent plastic materials. American Society for Testing and Materials, 2001.
10. Haertling GH. PLZT electro-optic materials and applications: a review. *Ferroelectrics* 1987;**75**:25–55.
11. Benkelfat BE, Horache EH, Zou Q, Vinouze B. An electro-optic modulation technique for direct and accurate measurement of birefringence. *Opt Commun* 2003;**221**:271–8.
12. Soh AK, Fang DN, Lee KL. Fracture analysis of piezoelectric materials with defects using energy density theory. *Int J Solids Struct* 2001;**38**:8331–44.
13. Lucato SL, Lupascu DC, Kamlah M, Rödel J, Lynch CS. Constraint-induced crack initiation at electrode edges in piezoelectric ceramics. *Acta Mater* 2001;**49**:2751–9.
14. Prume K, Gerber P, Kugeler C, Roelofs A, Bottger U, Waser R, et al. Simulation and measurements of the piezoelectric properties response (d_{33}) of piezoelectric layered thin film structures influenced by the top electrode size. In: *Proc 14th IEEE Int. Symp. App. Ferroelectr. ISAF-04, vol. 1*. 2004. p. 7–10.
15. So YW, Kim DJ, Noh TW, Yoon JG, Song TK. Polarization-switching mechanisms for epitaxial ferroelectric $Pb(ZrTi)O_3$ films. *J Korean Phys Soc* 2005;**46**:40–53.
16. Belov AY, Kreher WS. Micromechanics of ferroelectrics: from domain walls to piezoceramic devices. *Ferroelectrics* 2007;**351**:79–87.
17. Qiu W, Kang YL, Qin QH, Sun QC, Xu FY. Study for multilayer piezoelectric composite structure as displacement actuator by Moire interferometry and infrared thermography experiments. *Mater Sci Eng A* 2007;**452**:228–34.
18. Pane I, Fleck NA, Huber JE, Chu DP. Effect of geometry upon the performance of a thin film ferroelectric capacitor. *Int J Solids Struct* 2008;**45**:2024–41.
19. Liu QD, Fleck NA, Huber JE, Chu DP. Birefringence measurements of creep near an electrode tip in transparent PLZT. *J Eur Ceram Soc* 2009;**29**:2289–96.
20. Zeng T, Dong XL, Mao CL, Zhou ZY, Yang H. Effects of pore shape and porosity on the properties of porous PZT 95/5 ceramics. *J Eur Ceram Soc* 2007;**27**:2025–9.
21. Hall DA, Evans JDS, Covey-Crump SJ, Holloway RF, Oliver EC, Mori T, et al. Effects of superimposed electric field and porosity on the hydrostatic pressure-induced rhombohedral to orthorhombic martensitic phase transformation in PZT 95/5 ceramics. *Acta Mater* 2010;**58**:6584–91.
22. Zhang HL, Li JF, Zhang BP. Microstructure and electrical properties of porous PZT ceramics derived from different pore forming agents. *Acta Mater* 2007;**55**:171–81.
23. Setchell RE. Shock wave compression of the ferroelectric ceramic $Pb_{0.99}(Zr_{0.95}Ti_{0.05})_{0.98}Nb_{0.02}O_3$. *J Appl Phys* 2007;**101**:053525.
24. Belov AY, Kreher WS. Viscoplastic models for ferroelectric ceramics. *J Eur Ceram Soc* 2005;**25**:2567–71.
25. Sosa H. Plane problems in piezoelectric media with defects. *Int J Solids Struct* 1991;**28**:491–505.
26. Kumar S, Singh RN. Effect of the mechanical boundary condition at the crack surfaces on the stress distribution at the crack tip in piezoelectric materials. *Mater Sci Eng A* 1998;**252**:64–77.
27. Chen YH, Lu TJ. Cracks and fracture in piezoelectrics. *Adv Appl Mech* 2003;**39**:121–215.
28. Wang BL, Mai YW. On the electrical boundary conditions on the crack surfaces in piezoelectric ceramics. *Int J Eng Sci* 2003;**41**:633–52.
29. Dai L, Guo W, Wang X. Stress concentration at an elliptic hole in transversely isotropic piezoelectric solids. *Int J Solids Struct* 2006;**43**:1818–31.
30. Ou ZC, Chen YH. Re-examination of the PKHS crack model in piezoelectric materials. *Eur J Mech A/Solids* 2007;**26**:659–75.
31. Keve ET, Bye KL. Phase identification and domain structure in PLZT ceramics. *J Appl Phys* 1975;**46**:810–8.
32. Ivey M, Bolie VW. Birefringent light scattering in PLZT ceramics. *IEEE Trans Ultrason Ferroelectr Freq Contr* 1991;**38**:579–84.
33. Yao X, Chen Z, Cross LE. Polarization and depolarization behavior of hot-pressed lead lanthanum zirconate titanate ceramics. *J Appl Phys* 1983;**54**:3399–4003.
34. Viehland D, Li JF, Jang SJ, Cross LE, Wuttig M. Glassy polarization behavior of relaxor ferroelectrics. *Phys Rev B* 1992;**46**:8013–7.
35. Rauls MB, Dong W, Huber JE, Lynch CS. The effect of temperature on the large field electromechanical response of relaxor ferroelectric 8/65/35 PLZT. *Acta Mater* 2011;**59**:2713–22.
36. Glazer AM, Lewis JG, Kaminsky W. An automatic optical imaging system for birefringent media. *Proc R Soc Lond A* 1996;**452**:2751–65.
37. Liu QD, Huber JE. Inhomogeneous creep fields in PLZT: an experimental study. Proc SPIE 6929, 69290B; 2008. doi:10.1117/12.774385.
38. Belov AY, Kreher WS. Creep in soft PZT: the effect of internal fields. *Ferroelectrics* 2009;**391**:12–21.
39. Belov AY, Kreher WS. Simulation of microstructure evolution in polycrystalline ferroelectrics–ferroelastics. *Acta Mater* 2006;**54**:3463–9.